

LONG-TERM X-RAY CHANGES IN THE EMISSION FROM THE ANOMALOUS X-RAY PULSAR 4U 0142+61

M. E. GONZALEZ^{1,2}, R. DIB¹, V. M. KASPI^{1,3}, P. M. WOODS⁴, C. R. TAM¹, F. P. GAVRIIL⁵

Draft version November 16, 2018

ABSTRACT

We present results obtained from X-ray observations of the anomalous X-ray pulsar (AXP) 4U 0142+61 taken between 2000–2007 using *XMM-Newton*, *Chandra* and *Swift*. In observations taken before 2006, the pulse profile is observed to become more sinusoidal and the pulsed fraction increased with time. These results confirm those derived using the *Rossi X-ray Timing Explorer* and expand the observed evolution to energies below 2 keV. The *XMM-Newton* total flux in the 0.5–10 keV band is observed to be nearly constant in observations taken before 2006, while an increase of $\sim 10\%$ is seen afterwards and coincides with the burst activity detected from the source in 2006–2007. After these bursts, the evolution towards more sinusoidal pulse profiles ceased while the pulsed fraction showed a further increase. No evidence for large-scale, long-term changes in the emission as a result of the bursts is seen. The data also suggest a correlation between the flux and hardness of the spectrum, with brighter observations on average having a harder spectrum. As pointed out by other authors, we find that the standard blackbody plus power-law model does not provide the best spectral fit to the emission from 4U 0142+61. We also report on observations taken with the Gemini telescope after two bursts. These observations show source magnitudes consistent with previous measurements. Our results demonstrate the wide range of X-ray variability characteristics seen in AXPs and we discuss them in light of current emission models for these sources.

Subject headings: pulsars: general — pulsars: individual (4U 0142+61) — stars: neutron — stars: pulsar

1. INTRODUCTION

Recent observations of neutron stars have uncovered the wide variety of observational manifestations they appear to have, from rotation-powered pulsars and isolated thermally cooling objects to the so-called “magnetars” (see, Kaspi, Roberts & Harding 2006, for a review). The latter class includes Anomalous X-ray Pulsars (AXPs) and Soft Gamma Repeaters (SGRs; see Woods & Thompson 2006, for a review). Observationally, magnetars exhibit long spin periods of several seconds, have persistent X-ray luminosities of $\sim 10^{34-36}$ ergs s⁻¹ and have estimated surface dipolar magnetic fields of $0.6-7 \times 10^{14}$ G (see Kaspi 2007, for a recent review of AXPs). Optical and infrared (IR) counterparts have been found for many of these objects (e.g., Hulleman et al. 2001; Israel et al. 2003). Despite their soft spectrum at low X-ray energies, they have also been shown to produce copious amounts of hard X-ray emission (e.g., Molkov et al. 2004; Kuiper et al. 2006).

Magnetars are thought to be neutron stars whose X-ray emission is powered by the decay of an ultra-high magnetic field ($B > 10^{15}$ G; Thompson & Duncan 1995; Thompson & Duncan 1996; but see Bhattacharya et al. 2007). The sudden bursts of high-energy emission seen

from some of these sources are believed to be powered by the rearrangement of their magnetic field, while the nature of the optical/IR emission in this model is currently under study (Beloborodov & Thompson 2007). On the other hand, the active fallback disk model argues that the persistent emission at low X-ray energies arises from accretion onto the neutron star, while the optical/IR emission is thought to originate from the disk itself (e.g., Chatterjee et al. 2000; Alpar 2001). If only a passive (i.e. non-accreting) disk is present, it could then be responsible for part of the emission at optical/IR wavelengths (Wang et al. 2006). However, a magnetar origin for the high-energy bursts is still needed in all disk models, as well as a magnetospheric origin for any pulsed emission at optical/IR wavelengths. The large variety of unusual physical phenomena that high magnetic fields can power makes magnetars interesting objects to study.

4U 0142+61 is the brightest of all known AXPs. It has a period $P = 8.7$ s, period derivative $\dot{P} = 0.2 \times 10^{-11}$, inferred surface dipolar magnetic field strength of $B = 3.2 \times 10^{19} \sqrt{P\dot{P}}$ G = 1.3×10^{14} G, and has been detected from the mid-IR to hard X-rays (Israel et al. 1994; Gavriil & Kaspi 2002; den Hartog et al. 2007). In the mid-IR, Wang et al. (2006) have found evidence for a passive disk. The optical emission was found to be pulsed with a peak-to-peak pulsed fraction of $\sim 29\%$ (Kern & Martin 2002; Dhillon et al. 2005). Durant & van Kerkwijk (2006a) have derived a distance to the source of 3.8 ± 0.4 kpc. In addition, 4U 0142+61 has a soft X-ray spectrum that has been fitted traditionally with a blackbody plus power-law model with temperature $kT \sim 0.4$ keV and photon index $\Gamma \sim 3.3$ (e.g.,

¹ Department of Physics, Rutherford Physics Building, McGill University, 3600 University Street, Montreal, QC H3A 2T8, Canada.

² gonzalez@physics.mcgill.ca; NSERC PGS B.

³ Canada Research Chair in Observational Astrophysics, Lorne Trotter Chair in Astrophysics and Cosmology.

⁴ Dynetics, 1000 Explorer Blvd. Huntsville, AL 35806, USA; NSSTC, 320 Sparkman Drive, Huntsville, AL, 35805, USA

⁵ NASA Goddard Space Flight Center, Greenbelt, MD, USA; NPP Fellow, Oak Ridge Associated Universities, Oak Ridge, TN

Juett et al. 2002; Patel et al. 2003). However, the extrapolation of this soft X-ray model to the optical/IR overpredicts the observed emission if associated with the power-law component, while it underpredicts this emission if it is associated with the blackbody component.

A long-term monitoring campaign for 4U 0142+61 has been carried out with the *Rossi X-ray Timing Explorer* (*RXTE*) for the past 10 yrs. Using these data, Dib et al. (2007) reported a slow evolution of the pulse profile between 2000 and 2006, as well as a slow increase in the pulsed flux between 2002 and 2006. These changes may be associated with a possible glitch, or another event, that may have occurred between 1998–2000. Given the low amplitude of the reported variations, it is important to verify their presence with an independent instrument. In addition, the source appears to have entered an active phase showing three X-ray bursts in 2006 April–June and 2007 February (Kaspi et al. 2006; Dib et al. 2006; Gavriil et al. 2007a,b) which were followed up by various telescopes. The latter of these bursts is the longest and among the most energetic seen from AXPs to date (Gavriil et al. 2007b).

Therefore, constraining the long-term evolution of the emission from 4U 0142+61 is important for quantifying all AXP variability phenomena, in the hope of discovering correlations that can be checked against models, or uncovering phenomena common to all AXPs. Here we present results from observations of this source performed with *XMM-Newton*, *Chandra* and *Swift*, extending from 2000–2007. Indeed, long-term trends in the spectral and pulse characteristics are found, confirming the *RXTE* results, as well as changes coincident with the recent phase of burst activity. Observations in the near-IR after two of these bursts are also presented. We find that the overall evolution characteristics support a magnetar origin, while the detailed changes suggest that multiple emission mechanisms are likely present. The combined effect of these mechanisms is yet to be explored in current modeling of these sources.

2. X-RAY OBSERVATIONS

2.1. *XMM-Newton*

4U 0142+61 was observed seven times with *XMM-Newton* between 2002 and early 2007. The details of the observations are summarized in Table 1. We concentrated on data from the EPIC PN instrument (Turner et al. 2001) as it provided the best combination of longest time baseline and highest number of counts, in order to study the long-term evolution of the source with high precision.

All *XMM-Newton* observations were reduced and analyzed with SAS v7.0.0 and the latest calibration files available as of 2007 March. Periods of high particle background were excluded in the analysis and standard reduction techniques applied. The PN observations performed in the imaging small-window mode had a time resolution of 6 ms, while the ones in timing mode had a resolution of 0.03 ms. For the imaging observations, a circle of 40'' radius was used to extract the source counts. For the data in timing mode, the source events were extracted from a region 20 pixels wide around the source position. Background regions were chosen from regions in the same chip away from the source. The total number

TABLE 1
OBSERVATIONS OF 4U 0142+61

Date	MJD	CCD Mode/Exp. Time	Counts ^a
<i>XMM-Newton</i> :			
13/02/2002	52318.3	Small-Window/2.9 ks	1.29×10 ⁵
24/01/2003	52663.9	Small-Window/3.8 ks	1.62×10 ⁵
01/03/2004	53065.5	Timing/29.4 ks	1.47×10 ⁶
24/07/2004	53211.3	Timing/21.2 ks	1.07×10 ⁶
28/07/2006	53944.8	Small-Window/3.7 ks	1.71×10 ⁵
13/01/2007	54113.8	Small-Window/4.4 ks	1.95×10 ⁵
10/02/2007	54141.1	Timing/8.6 ks	4.24×10 ⁵
<i>Chandra</i> :			
21/05/2000	51685.8	Continuous Clocking/5.9 ks	1.23×10 ⁵
29/05/2006	53915.4	Continuous Clocking/18.6 ks	3.86×10 ⁵
10/02/2007	54141.3	Continuous Clocking/20.1 ks	3.99×10 ⁵
<i>Swift</i> :			
13/02/2005	53414.8	Windowed-Timing/6.6 ks	2.8×10 ⁴
10/02/2007	54141.2	Windowed-Timing/3.5 ks	1.6×10 ⁴

^a Net counts in the 0.5–10 keV range. Uncertainties smaller than last digit shown.

of background-subtracted counts detected for each observation are shown in Table 1. While the *XMM-Newton* count rates in each observation are ~ 45 cts s⁻¹, the fast read-out modes in which the instruments were operated prevented pileup problems.

2.2. *Chandra*

4U 0142+61 has been observed three times with *Chandra* at sufficiently high time resolution to allow useful timing studies (see Table 1). The ACIS Continuous Clocking (CC) mode allows for 2.9 ms resolution at the expense of one dimension of spatial resolution. The effects of pileup are negligible in this mode. The data were reduced using CIAO v3.3.0 and standard techniques⁶. Source events were extracted from a region 4 pixels wide ($\sim 2''$) around the peak of the emission, with background regions taken far from the source.

2.3. *Swift*

4U 0142+61 has been observed numerous times with *Swift*. For the purpose of our work, we chose the X-ray Telescope (XRT) observations with the highest number of counts and sufficiently high time resolution to allow for a study of the timing properties of the pulsar (see Table 1). The data were reduced applying standard screening criteria and using *Swift* Software v2.5a under HEASoft v6.1.1. Source counts were extracted in regions 60 pixels ($\sim 2.4''$) wide around the peak of the emission, with background regions taken far from the source. We only considered events with grade 0 to improve spectral resolution and used the latest redistribution matrices (v008).

3. X-RAY PULSE RESULTS

3.1. *Pulse Profiles*

The *XMM-Newton*, *Chandra*, and *Swift* data were used to study the long-term evolution of the X-ray pulse

⁶ <http://cxc.harvard.edu/ciao/threads/aciscctoa/> and <http://wwwastro.msfc.nasa.gov/xray/ACIS/cctime>

profile. The data were transformed to the solar system barycenter and folded at the predicted periods for each observation using ephemerides derived from Dib et al. (2007). The data were divided into different energy ranges: 0.5–10, 0.5–2 and 2–10 keV. Sample background-subtracted, normalized pulse profiles for these bands are shown in Figure 1. Prior to 2006, an evolution of the pulse profile in the 2–10 keV band is clearly visible and confirms the results obtained using *RXTE* by Dib et al. (2007). In addition, the sensitivity to lower energies allows us to further constrain the evolution and conclude that it is also present in the 0.5–2 keV band.

More specifically, before 2006 we find that the relative height of the two peaks increased with time, while the depth of the dip between them became less pronounced. This caused the profiles to become more sinusoidal, as can be seen from a Fourier analysis, in which the ratio of the power in the first harmonic to the total power increased while this same ratio for the second harmonic stays fairly constant. Figure 2 shows these ratios for the profiles in the 2–10 keV range obtained from both *XMM-Newton* and *RXTE* (see Dib et al. 2007, for details). The ratio of power in the higher harmonics then decreases during this time. Given that *RXTE* profiles before the bursts were derived by averaging many observations to increase the signal-to-noise ratio, the fact that a similar evolution is seen in the individual *XMM-Newton* observations confirms the long-term nature of the observed changes. The *Chandra* and *Swift* profiles (not shown in Fig. 2) show similar results. After the bursts were detected in 2006, the profiles fluctuate more (with more power going to higher harmonics around the time of the bursts, see also Gavriil et al. 2007b) and the overall evolution towards more sinusoidal profiles seems to have ceased.

3.2. Pulsed Fractions

The fact that the pulse profile evolves with time makes it difficult to determine the pulsed fractions (and thus pulsed fluxes) of the source accurately. A few different methods are commonly used in the literature to calculate these values; each has advantages and caveats (see Archibald et al. 2007, in preparation). Here we compare the results obtained from two of these methods: the root-mean-square (RMS) and area methods.

We calculate the RMS pulsed fraction using:

$$PF_{rms} = \frac{\sqrt{2\sum_{k=1}^n ((a_k^2 + b_k^2) - (\sigma_{a_k}^2 + \sigma_{b_k}^2))}}{\frac{1}{N}\sum_{i=1}^N p_i} \quad (1)$$

where a_k is the k^{th} even Fourier component defined as $a_k = \frac{1}{N}\sum_{i=1}^N p_i \cos(2\pi ki/N)$, $\sigma_{a_k}^2$ is the uncertainty of a_k , b_k is the odd k^{th} Fourier component defined as $b_k = \frac{1}{N}\sum_{i=1}^N p_i \sin(2\pi ki/N)$, $\sigma_{b_k}^2$ is the uncertainty of b_k , i refers to the phase bin, N is the total number of phase bins, p_i is the count rate in the i^{th} phase bin of the pulse profile, and n is the maximum number of Fourier harmonics to be taken into account (we have used 5 harmonics for 4U 0142+61, see also Dib et al. 2007). On the other hand, the area pulsed fraction is obtained using:

$$PF_{area} = \frac{\frac{1}{N}\sum_{i=1}^N (p_i - p_{min})}{\frac{1}{N}\sum_{i=1}^N p_i} \quad (2)$$

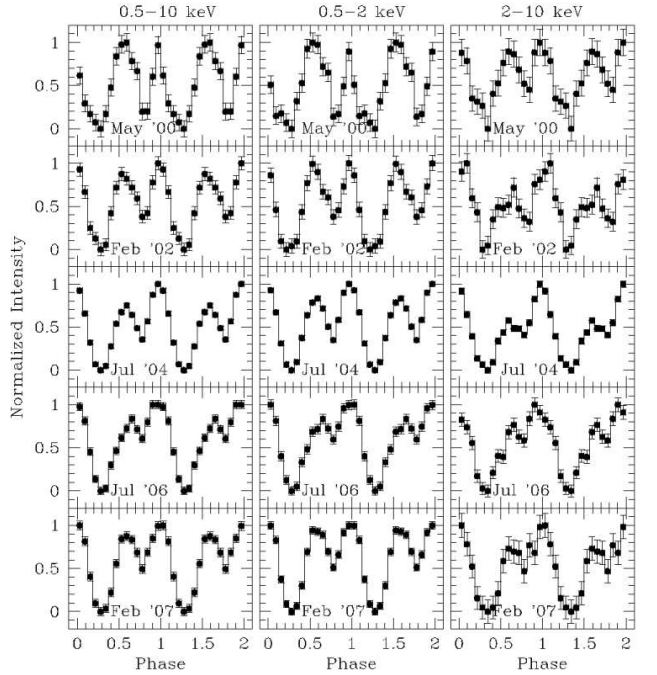


FIG. 1.— Sample pulse profiles for 4U 0142+61 in the 0.5–10 keV (*left*), 0.5–2 keV (*center*) and 2–10 keV (*right*) ranges. The profiles have been normalized to have minimum and maximum values between 0 and 1. The top profiles (2000 May) were obtained with *Chandra*, and the rest with *XMM-Newton*. The two bottom profiles were taken after the burst activity was first detected.

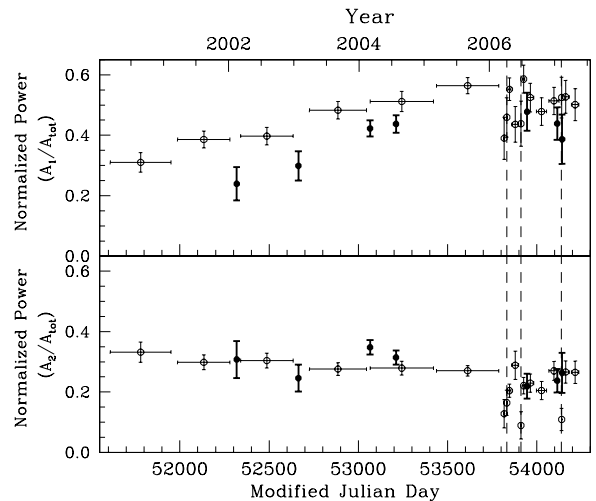


FIG. 2.— Fourier amplitudes of the pulse profiles using *XMM-Newton* (bold, solid points) and *RXTE* (simple points) in the 2–10 keV band. The pre-burst *RXTE* points are taken from Dib et al. (2007). The dashed lines indicate the three burst epochs. *Top*: Ratio of the Fourier amplitude of the fundamental to that of the power in all Fourier amplitudes. *Bottom*: Ratio of the Fourier amplitude of the second harmonic to that of the power in all Fourier amplitudes.

where p_{min} is the average count rate in the “minimum” phase bins of the profile (as determined by cross-correlating with a high signal-to-noise template).

While least sensitive to noise, the RMS method returns a pulsed flux number that is affected by pulse pro-

file changes. On the other hand, while the area method is more physically meaningful, problems in locating the true minimum and its error because of noise and binning tend to bias these values upward. Various recommendations have been made in order to derive a better estimate for the pulsed fractions for each of these methods (Archibald et al. 2007, in preparation) which we have applied here. The resulting values for all the observations of 4U 0142+61 listed in Table 1 are shown in Figure 3. We note that the *Chandra* values appear to be consistently lower than those found using *XMM-Newton* and *Swift* and could reflect the calibration uncertainties present in these data (see below).

A significant change in the pulsed fraction over time is seen for both methods. Overall, the pulsed fraction has increased with time, reaching an apparent maximum in the observations taken after the 2006 burst activity from the source. For example, using the values from the RMS (area) method, the pulsed fraction measured with *XMM-Newton* between 2002 and 2006 has increased by $40\pm 8\%$ ($58\pm 12\%$), $28\pm 9\%$ ($57\pm 15\%$) and $35\pm 14\%$ ($63\pm 22\%$) in the 0.5–10, 0.5–2 and 2–10 keV bands, respectively. The pulsed fraction also increased significantly in the pre-burst observations (2002–2004) and between the observations taken before and after the bursts were first detected (2004–2006): in the 0.5–10 keV range, the RMS (area) increase was $23\pm 6\%$ ($27\pm 7\%$) and $14\pm 4\%$ ($25\pm 7\%$) during these time periods, respectively.

In addition, we find evidence for an increase in pulsed fraction with energy in the longest *XMM-Newton* observations: in the 0.5–1 keV and 6–10 keV ranges we find RMS values of $5.1\pm 0.3\%$ and $14\pm 2\%$, respectively. However, when using the area method we find values of $7.9\pm 0.6\%$ and $18\pm 5\%$ at 0.5–1 keV and 6–10 keV, respectively. Given that the pulse profile changes significantly with energy and the area method gives less significant changes, we view this suggestive increase in pulsed fraction with energy with caution.

4. X-RAY SPECTRAL RESULTS

The spectra were binned to contain a minimum of 50 counts per spectral channel. For the *XMM-Newton* PN data, due to the large number of counts collected from these observations, the statistical errors are very small and a systematic error of 2% was added to each spectrum (consistent with current calibration uncertainties in the PN, Kirsch et al. 2004). The phase-averaged PN spectrum for each observation was fitted in the 0.6–10 keV range using the XSPEC package v.11.3.0. Unfortunately, we cannot make use of the *Chandra* observations taken in CC mode to study the spectral characteristics of 4U 0142+61. While the *XMM-Newton* observations confirm that spectral changes are present in the source at the $\sim 10\%$ level (as will be shown below), the CC data show variations at levels higher than this, which cannot be corrected for at present due to calibration uncertainties⁷. The lower signal-to-noise *Swift* XRT data do not contribute to constraining the evolution of the spectrum, other than to suggest that changes are present. Therefore, the *XMM-Newton* PN was used as the prime instrument to study the long term spectral evolution of

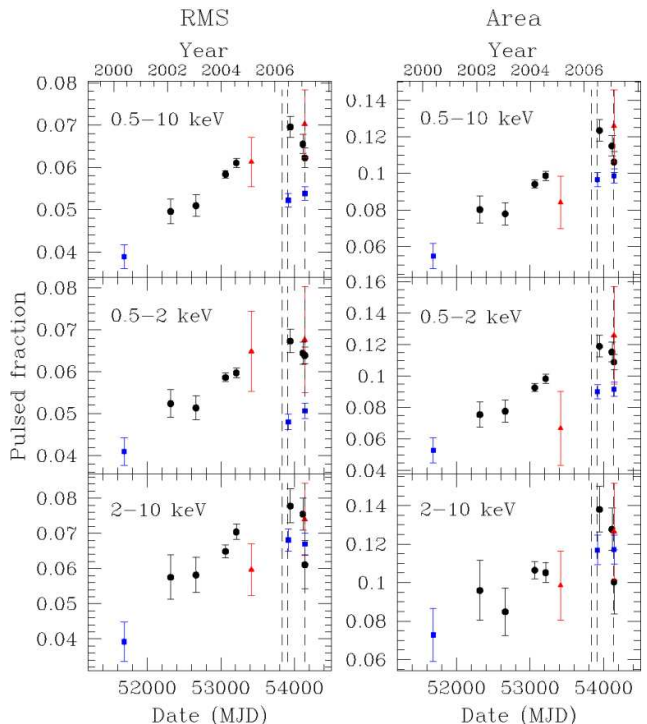


FIG. 3.— RMS (left) and area (right) pulsed fractions in the 0.5–10 keV (top), 0.5–2 keV (center) and 2–10 keV (bottom) ranges. Values shown correspond to those measured with *XMM-Newton* (black circles), *Chandra* (blue squares) and *Swift* (red triangles). The dashed lines indicate the three burst epochs.

4U 0142+61.

The *XMM-Newton* PN spectra were fitted simultaneously assuming a common value for the column density N_H , which was then held constant at its best-fit value. As previously reported, single-component models do not describe the emission well and we tried various multi-component models, as listed in Table 2 and shown in Figure 4. Rea et al. (2007a,b) have used various models to fit the emission from 4U 0142+61 in the 1–250 keV range. Güver et al. (2007) have also used a spectral model based on a variant of the magnetar model to fit the *XMM-Newton* data from 4U 0142+61. Our fits below are as statistically acceptable as those presented by these authors. In addition, although the main focus of our paper is to report on the long-term evolution of the emission, we point out that the specific values for temperature, emitting area, unabsorbed flux etc. depend heavily on the model that is used to describe this emission. This dependence can be seen by comparing the parameter values shown in Table 2 and the unabsorbed fluxes shown in Figures 5 and 6. We will therefore concentrate on flux changes that are seen to be model-independent.

4.1. Phase-averaged Spectrum

The traditional blackbody plus power-law model used for AXPs (BB+PL) gives results consistent with those previously reported for the source (e.g., Juett et al. 2002, Patel et al. 2003). However, the derived null probability is close to zero and many features are evident in the residuals (see Fig. 4). In addition, the derived value for the column density of interstellar absorption for this model is

⁷ See CXC Helpdesk ticket #9114

inconsistent with that estimated by Durant & van Kerkwijk (2006) based on the analysis of the high-resolution RGS spectra available from the longer *XMM-Newton* observations listed in Table 1 ($N_H = (6.4 \pm 0.7) \times 10^{21} \text{ cm}^{-2}$).

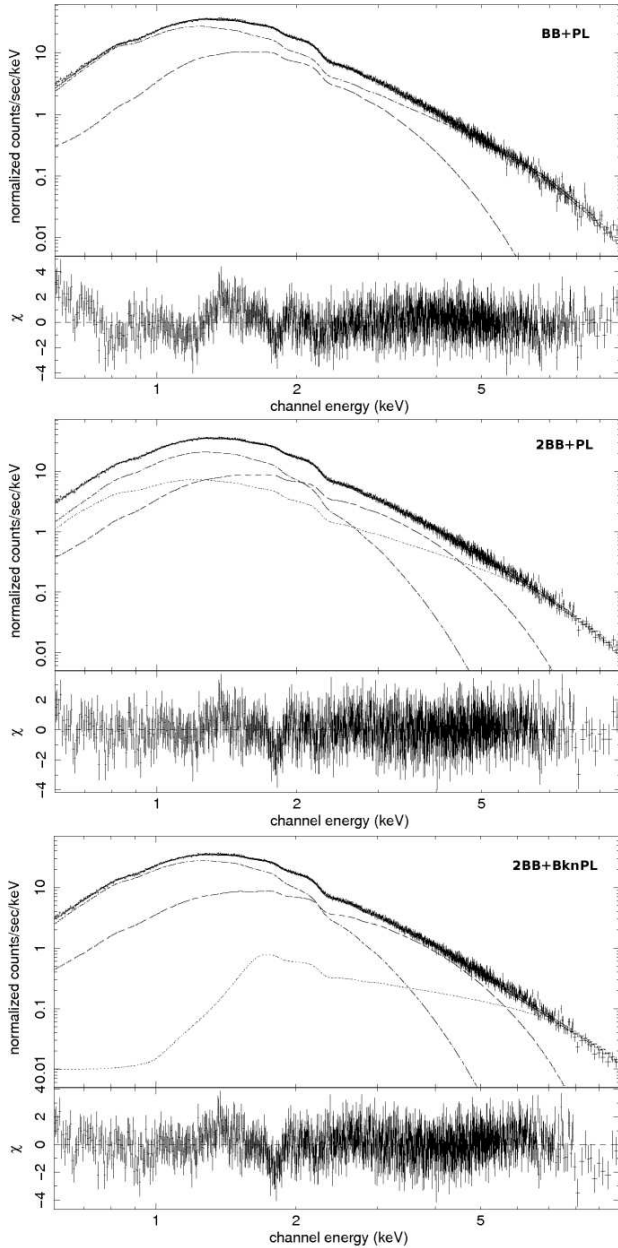


FIG. 4.— Best-fit spectral models and residuals obtained for the representative 2004 March *XMM-Newton* observation of 4U 0142+61. The models shown are BB+PL (top), 2BB+PL (middle) and 2BB+BknPL (bottom). See Table 2 for fit values. The individual components for each model are also shown.

A two-blackbody model does not fit the observed spectrum well. Instead, a two-blackbody plus power-law model (2BB+PL) produces the best statistical fit to the data from our sample of models. The properties of the two blackbody components could correspond to that of a cool component with large emitting area and a hot component with small area. The range of temperature and emission area values are consistent with

TABLE 2
SUMMARY OF SPECTRAL FITS TO THE *XMM-Newton* SPECTRA
(SEE §4 FOR DETAILS)

Parameter ^a	Range of values ^b
<i>Blackbody+Power-law (BB+PL):</i>	
N_H	$9.8(2) \times 10^{21} \text{ cm}^{-2}$
kT	$0.391(9) - 0.44(1) \text{ keV}$
R (km)	$5.7(7) - 7.3(8) \text{ km}$
Γ	$3.69(7) - 3.771(8)$
$\chi^2(\text{dof})$	7407(6843)
Probability	1.1×10^{-6}
<i>2 Blackbodies+Power-law (2BB+PL):</i>	
N_H	$7.0(2) \times 10^{21} \text{ cm}^{-2}$
kT_{cool}	$0.295(9) - 0.31(1) \text{ keV}$
R_{cool}	$14(2) - 16(2) \text{ km}$
kT_{hot}	$0.53(1) - 0.57(2) \text{ keV}$
R_{hot}	$2.9(9) - 3.8(6) \text{ km}$
Γ	$2.76(9) - 2.95(8)$
$\chi^2(\text{dof})$	6558(6834)
Probability	0.991
<i>2 Blackbodies+Broken Power-law (2BB+BknPL):</i>	
N_H	$6.0(1) \times 10^{21} \text{ cm}^{-2}$
kT_{cool}	$0.27(1) - 0.32(1) \text{ keV}$
R_{cool}	$15(1.6) - 19(2.5) \text{ km}$
kT_{hot}	$0.52(3) - 0.61(2) \text{ keV}$
R_{hot}	$2.5(3) - 4.4(9) \text{ km}$
Γ	$1.42(5) - 1.73(4)$
$\chi^2(\text{dof})$	6777(6834)
Probability	0.684

^a kT and R represent the observed blackbody temperature and radius, respectively, while Γ is the power-law photon index.

^bErrors quoted are 1σ confidence level. Radii calculated using a distance of $3.8 \pm 0.4 \text{ kpc}$. Not in chronological order.

emission from the surface of a neutron star. From current magnetar theory, thermal emission from the surface is expected to be scattered in the magnetosphere to produce high-energy emission above the thermal peak (Thompson et al. 2002). To simulate this behavior, we have also fit a blackbody plus broken power-law model to the data, where the “break” energy is set to be the peak of the blackbody model. In addition, the power-law component is manually set to contribute negligible emission below this peak while having a freely-varying photon index above the peak. In this case, we find that a single blackbody model cannot reproduce the spectral shape at low energies. Adding another blackbody model significantly improves the fit (2BB+BknPL). Plots of these models to the spectrum for the 2004 March observation are shown in Figure 4 as an example⁸.

A summary of the range of values for all the observations obtained from these fits is shown in Table 2. The high quality data used here expand on what has already been pointed out by other authors: in addition to the dubious physical nature of the standard blackbody plus power-law model used to fit AXP spectra, the data suggest that statistically speaking, it does not reproduce the observed spectra well, at least for 4U 0142+61. While we

⁸ Due to the high statistics, the data show residuals at $\sim 1.8 \text{ keV}$ that coincide with a Silicon edge in the PN effective area calibration (<http://xmm.vilspa.esa.es/docs/documents/CAL-TN-0018.pdf>)

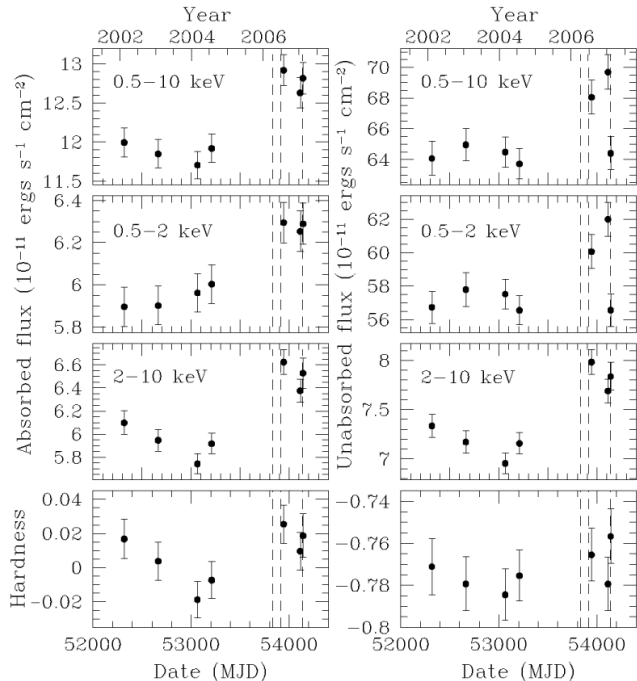


FIG. 5.— Phase-averaged fluxes and hardness ratios derived for the BB+PL model. Absorbed (*left*) and unabsorbed (*right*) values are shown. The dashed lines indicate the three burst epochs.

cannot claim that the models presented here are better physical representations of the observed emission than those presented by, e.g., Güver et al. (2007), they describe the observed spectral shape better than a BB+PL and produce reasonable spectral parameters.

Independent of the model used to fit the data, we find significant changes in the spectral characteristics of 4U 0142+61 during the span of the observations. Figure 5 shows the absorbed and unabsorbed fluxes, as well as the hardness of the spectrum, derived using the BB+PL fit. The hardness is calculated using $(H - S)/(H + S)$, where S is the flux in the 0.5–2 keV range and H is the flux in the 2–10 keV range. The values for the unabsorbed flux as given by the 2BB+PL and 2BB+BknPL fit are shown in Figure 6. Overall, before the recent burst activity, the total flux was fairly constant, with a possible decrease in flux being present and accompanied by an overall softening. After the 2006 burst activity, this trend reversed and we find that the 0.5–10 keV flux increased by $(10 \pm 3)\%$. The increase in flux is also energy dependent, with the 0.5–2 and 2–10 keV ranges showing increases of $(7 \pm 3)\%$ and $(15 \pm 3)\%$, respectively. In addition, the spectra for the two observations carried out close to burst epochs show evidence of hardening, while the one in between shows a softer spectrum. These results are independent of the spectral model used to fit the data.

The reported fluxes include a 2% error due to calibration uncertainties, which greatly dominates over statistical errors due to the large number of counts detected. We also find that the observed flux variability is mainly caused by changes in the observed PN count rate of the source and not uncertainties in the calibration of the instrumental response. An almost identical long-term be-

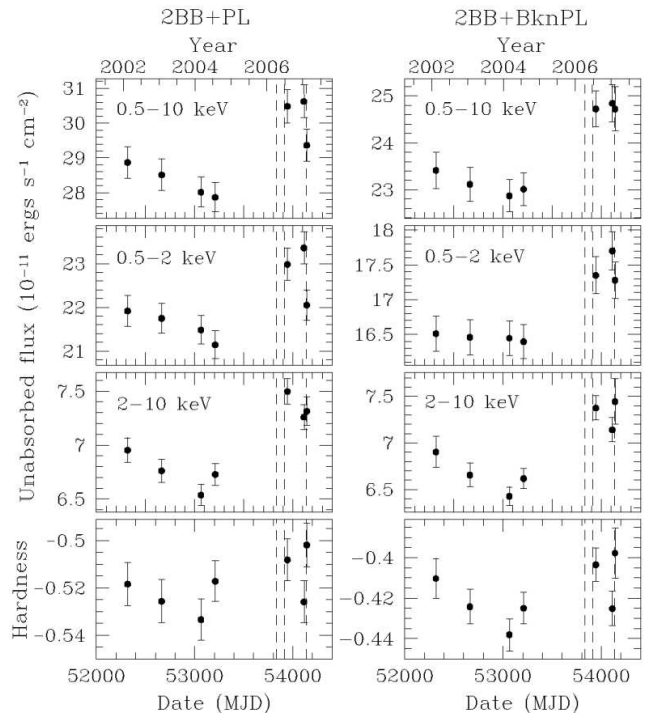


FIG. 6.— Phase-averaged unabsorbed fluxes and hardness ratios derived for the 2BB+PL (*left*) and 2BB+BknPL (*right*) model. The dashed lines indicate the three burst epochs.

havior in the count rate and flux is measured with MOS1 (operated in timing mode in all but the last observation), albeit with large cross-calibration offsets with respect to the PN instrument and smaller number of counts. The MOS2 chips were operated in three different modes during 6 of these observations (it was turned off on 2002 February), with two imaging observations also showing an increase in the flux. Thus, we argue that the observed spectral changes are intrinsic to 4U 0142+61 and not dominated by calibration uncertainties.

We also find that the hardness of the spectrum is determined mainly by the flux at higher energies, and not necessarily by the spectral properties described by model parameters such as temperature and photon index (which are also very dependent on the model used to fit the spectrum). This is shown in Figure 7 using the values derived from the 2BB+BknPL model (as it is the most magnetar-inspired of the models used), where we find that the hardness versus flux data (top) deviate from a constant at the 2.7σ level while the photon index (bottom) is consistent with being constant. Similar results are obtained for the blackbody temperatures where, if anything, their values are slightly lower for observations taken after 2006 when the flux was higher and the spectrum was harder.

4.2. Pulsed Flux

We also studied the changes in pulsed flux during the observations, the values of which can be compared to those derived from the *RXTE* observations presented by Dib et al. (2007). We have estimated the pulsed flux for each observation by taking the phase-averaged flux calculated above and multiplying it by the pulsed frac-

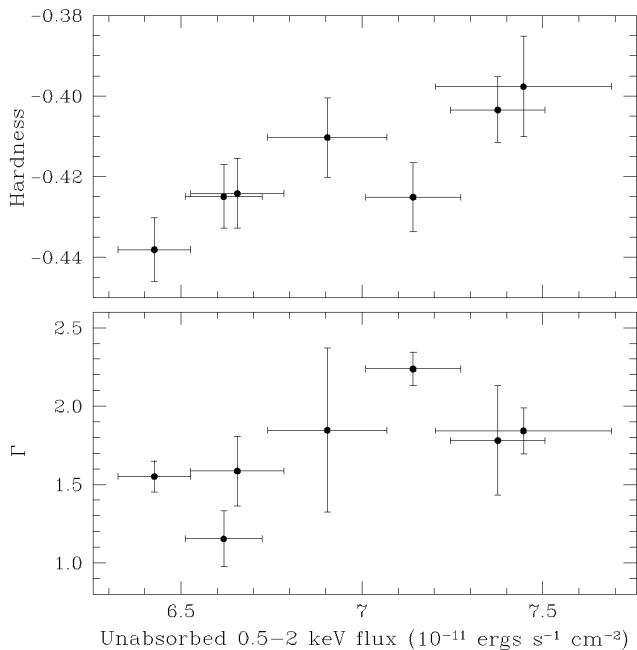


FIG. 7.— Hardness versus flux from the *XMM-Newton* observations as given by the 2BB+BknPL model. Absorbed (*top*) and unabsorbed (*bottom*) fluxes in the 2–10 keV range are shown. The hardness is derived using $(H - S)/(H + S)$, where H is the flux in the 0.5–2 keV range and S is the flux in the 2–10 keV range.

tion derived in §3.2 using the area method. The pulsed flux for each observation derived from the 2BB+BknPL model is shown in Figure 8 (using the absorbed flux, as strictly speaking only an “absorbed pulsed fraction” can be measured). Similarly, in Figure 9 we plot the absorbed pulsed flux in the 2–10 keV range derived from *RXTE* observations. Figure 9 is an updated version of that found in Dib et al. (2007) and is extended to include the most recent observations of 4U 0142+61. The flux in counts and energy are both shown, as the former allows for higher time resolution (the observations where bursts were seen are denoted with stars), while the latter combines multiple observations and allows for direct comparison with the lower panel of Figure 8 (see Dib et al. 2007; Gavriil et al. 2007b, for details). As can be seen from both Figures, the same long-term trend is present in both data sets, albeit *XMM-Newton* has larger uncertainties at 2–10 keV due to its lower sensitivity in this energy range and the smaller number of observations available. The apparent offset between the *RXTE* and *XMM-Newton* fluxes at 2–10 keV is likely caused by cross-calibration uncertainties.

5. INFRARED OBSERVATIONS

5.1. *Gemini*

Two Director’s Discretionary Time (DDT) observations of 4U 0142+61 were obtained with the *Gemini* North Telescope, on 2006 June 30 and 2007 February 13. Both observations were taken 5–6 days after an X-ray burst (Dib et al. 2006; Gavriil et al. 2007a). K_S -band images were made with the Near-Infrared Imager (NIRI), an ALADDIN InSb 1024×1024 pixel detector ar-

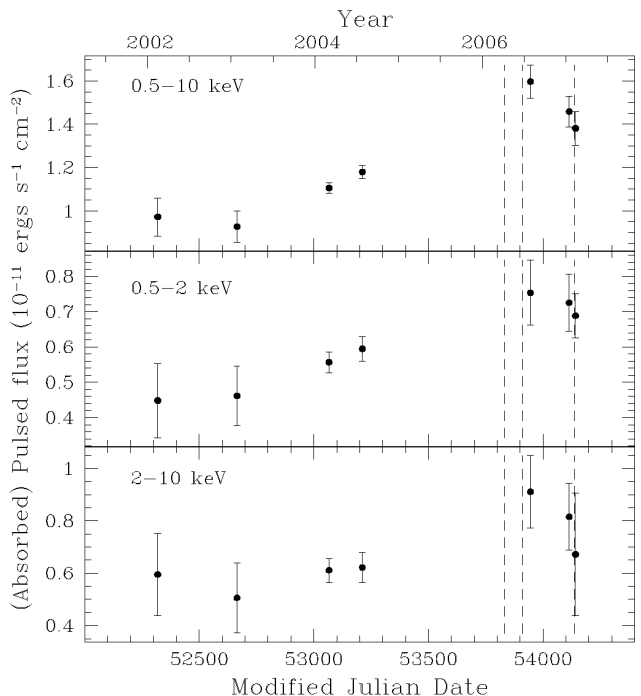


FIG. 8.— Pulsed fluxes for 4U 0142+61 obtained from the absorbed fluxes for the 2BB+BknPL model and the pulsed fraction derived using the area method. The dashed lines indicate the three burst epochs.

ray which, with the f/6 camera, provided a 119.9×119.9 arcsec² field of view and plate scale of $0''.117$ per pixel. The standard reduction procedures were performed using the *Gemini* package (v1.6) for IRAF (v2.12.2). Each frame was a 2×30 s integration; 17 dithered frames in 2006 June and 20 in 2007 February, were averaged to make one combined image for each observation.

5.2. Results

The point source 4U 0142+61 was clearly identified in both *Gemini* observations. We used DAOPHOT in IRAF for point spread function (PSF) photometry; the FWHM of the PSF was approximately $0''.5$ on 2006 June 30 and $0''.6$ on 2007 February 13. Using the results of Hulleman et al. (2004), we calibrated our photometry relatively by measuring the K_S -band magnitude offsets of 10 nearby field stars and applying that offset to the 4U 0142+61 counterpart, incorporating the offset scatter into the final uncertainties. The final calibrated magnitudes are $K_S = 19.70 \pm 0.05$ and $K_S = 19.86 \pm 0.05$ mag in 2006 June and 2007 February, respectively. The uncertainties are DAOPHOT-determined and include the calibration uncertainties.

Observations of 4U 0142+61 before the bursts have encompassed a large magnitude range, from $K = 19.68 \pm 0.05$ to $K' = 20.78 \pm 0.08$ mag (Hulleman et al. 2004; Durant & van Kerkwijk 2006c), consistent with the above values measured after the bursts. Therefore, we find no evidence to suggest that the AXP had brightened significantly in the near-IR several days after the X-ray bursts.

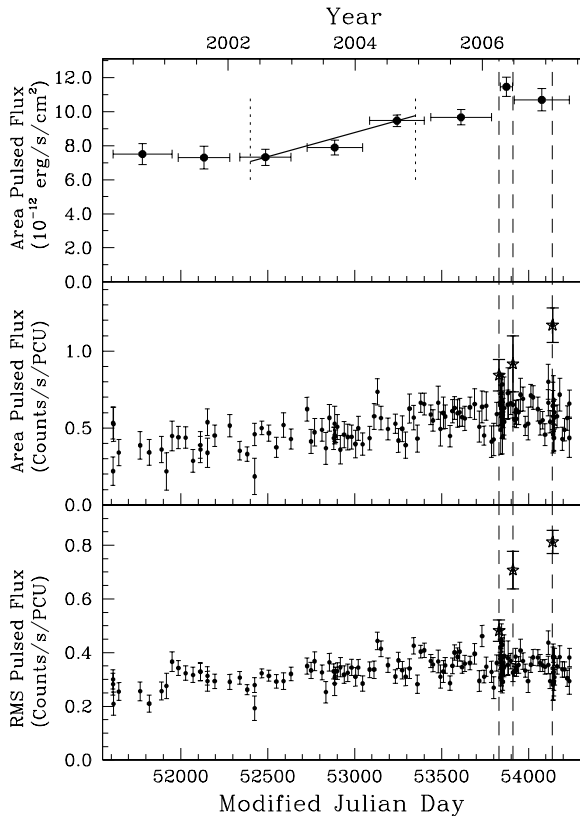


FIG. 9.— Pulsed fluxes for 4U 0142+61 in the 2–10 keV range obtained using *RXTE*. Fluxes in counts derived using the area (*center*) and RMS (*bottom*) methods are shown for individual observations (those where bursts were seen are denoted with stars and dashed lines). Fluxes in energy (*top*) are absorbed and were obtained by combining multiple observations and fitting the resulting spectra using XSPEC. The sloped line (bounded by the two short dashed lines) shows the $\sim 29\%$ pulsed flux increase reported in Dib et al. (2007).

6. DISCUSSION

We have found that the X-ray emission from 4U 0142+61 changed significantly from 2000–2007. Before the 2006 burst activity, the pulse profile became more sinusoidal and the pulsed fraction (and pulsed flux) increased. Our results agree with those of Dib et al. (2007) reported in the 2–10 keV range using *RXTE* data and we find that these changes are also present in the 0.5–2 keV band. During this time, the total flux was approximately constant with time (although a slight decrease is suggested depending on the spectral model used). The emission also showed an overall softening independent of the assumed spectral model. After 2006, the total flux in the 0.5–10 keV range increased by $\sim 10\%$ while the spectrum hardened for those observations close to the detected bursts (the spectrum softened in between these observations). The flux increase after the bursts is also energy-dependent, with higher energies showing a larger increase. During this time, the pulse profile evolution towards more sinusoidal shapes stopped and the pulsed fraction was higher than before. We also find that in general, changes in flux and hardness of the spectrum appear to be correlated, with observations having a

higher flux also showing a harder spectrum. This correlation appears to hold at least for the small range of flux phase-space that is covered by the current observations. In addition, the softening of the spectrum before 2006 agrees with the results presented by Dib et al. (2007) and the spectral hardening for observations close to detected bursts (in addition to a softening in between) agrees with the behavior observed by Gavriil et al. (2007b). Our pre-burst absorbed fluxes also agree with those of Rea et al. (2007a) reported using a BB+PL model.

Anomalous X-ray pulsars exhibit a wide range of behavior in their variability, from sudden energetic bursts to long-term changes. The AXP 1E 1048–5937 was shown to have large, long-term flares of its pulsed flux (one of them lasting about a year, Gavriil & Kaspi 2004) and variations by a factor of $\gtrsim 2$ to its phase-averaged flux (Tiengo et al. 2005). This source has recently become active again, causing prolonged changes to its observed emission and showing a correlation between hardness and flux as seen here for 4U 0142+61 (Tam et al. 2007). Changes in the phase-averaged flux of 1RXS J170849.0–400910 of $\sim 60\%$ on a timescale of years have also been reported (Campana et al. 2007) with a correlation between hardness and flux as well (albeit using various telescopes and instruments). 1RXS J170849.0–400910 was shown to have pulse profile changes possibly associated with glitches and low-level pulsed flux variations at various epochs, while 1E 1841–045 was shown to have possible long-term pulse profile changes and glitches with no obvious radiative changes (Dib et al. 2007). On the other hand, a large outburst accompanied by long-term changes in almost all emission characteristics was seen in 1E 2259+586 that also shows a hardness–intensity correlation⁹ (Kaspi et al. 2003; Woods et al. 2004; Zhu et al., in preparation).

The very low-level, long-term spectral changes seen here for 4U 0142+61 have not been observed thus far in other sources and were detected thanks to the high quality of the available data. The fact that the largest changes are suggested to be accompanied by bursting activity point to a common magnetar origin (see below). The overall changes in pulse and spectral properties of 4U 0142+61 support the view of magnetars as very active sources with a wide range of variability characteristics. We now discuss the observed changes in light of the commonly cited models for AXP emission: the magnetar and disk models.

6.1. The Magnetar Model

In the magnetar model, thermal X-ray emission from the surface provides seed photons which are resonantly Compton-scattered (RCS) to higher energies by the enhanced currents in a twisted magnetosphere (Thompson et al. 2002; Lyutikov & Gavriil 2006; Fernández & Thompson 2007). It is also expected that additional thermal emission will be produced by re-

⁹ We note that a BB+PL model to the observed emission from these sources results in large temperatures and steep power-law indices. As such, the power-law component may in fact dominate the observed emission below ~ 1 –2 keV, as shown in Figure 4 for 4U 0142+61. Therefore, the hardness–intensity correlations that are measured in terms of the value of the power-law index may be dominated by the evolution of the low-energy emission from these sources.

turn currents from the magnetosphere that heat the surface. In turn, bursts of emission are explained as sudden, small-scale reconfigurations of the surface following a crustal yield due to a magnetospheric twist. Large outbursts are explained as global reconfigurations and/or reconnections of the magnetic field after a large twist. Long-term variability, assuming constant underlying thermal emission, is viewed as increases (or decreases) in the twisting of the magnetosphere by currents from the stressed crust. The optical depth to scattering increases as the twist angle of the magnetosphere increases and in this case we expect a hardening of the spectrum to accompany an increase of the emitted flux. This scenario has been used to explain the hardness–intensity correlation observed in magnetars. The fact that the predicted correlation between flux and hardness is seen for 4U 0142+61 (with the brighter observations having a harder spectra) and that the largest changes are observed to coincide with a period of increased burst activity supports this interpretation.

Özel & Güver (2007) have proposed that the hardness–intensity correlation observed in the afterglow emission from magnetars arises mainly from the cooling crust of the star and less so from changes in the magnetospheric currents. For example, most of the burst emission (arising from a large twist in the magnetosphere) can be deposited deep in the crust¹⁰, heating it, and its subsequent cooling dominates the spectral evolution of the star. In this case, the observed temperature and total flux would have a direct correlation and could explain the hardness–intensity correlation.

However, this does not seem to be the case for 4U 0142+61. While the latest burst observed from it was the longest and among the most energetic detected from AXPs thus far (Gavriil et al. 2007a,b), all observations taken after the burst show a rapid return to the previous state without additional changes. This suggests that long-term recovery regions (e.g., the inner crust) have not been significantly affected, or that they were slightly affected and recovered very quickly. In either case, the bulk of the long-term changes observed after the bursts would be mainly magnetospheric in origin. This is supported by the fact that the main spectral changes appear to be dominated by the emission above 2 keV and that the evolution towards simpler, more sinusoidal profiles appears to have ceased.

We also note that the long-term evolution of the pulsed fraction in 4U 0142+61 does not show a simple correlation with the total flux. This is different from what is observed other sources, such as 1E 2259+586, 1E 1048.1–5937 and 1RXS J170849.0–400910, where larger phase-averaged fluxes correspond to lower pulsed fractions (Woods et al. 2004; Tiengo et al. 2005; Tam et al. 2007). The behavior of these AXPs could be accounted for, at least in principle, as a growing hot spot on the surface. In the transient AXP XTE 1810–197, as the source slowly fades after a large (undetected) burst around the end of 2002, the pulsed fraction and flux both decrease with time. This behavior may be interpreted as a fading hot spot against the background of a large-area cool blackbody (Gotthelf & Halpern 2007).

¹⁰ Güver et al. (2007) estimate a heating depth of ~ 2.5 m for the outburst seen from the transient AXP XTE 1810–197.

However, in the case of 4U 0142+61 we see a continuous increase in the pulsed fraction independent of the total flux, suggesting that different mechanisms contribute to this emission with varying strengths over time. The twisted magnetosphere model generally predicts that pulsed fractions should correlate positively with twist angles (Fernández & Thompson 2007), and this mechanism could be responsible for the bulk of the increase during the observed bursting period. However, the continuous increase before the bursts is still hard to understand.

We then find that the emission from 4U 0142+61 shows distinct characteristics from those of other AXPs, and while it generally agrees with magnetar models, the complicated evolution of the emission characteristics requires more intricate mechanisms than are presently available.

The hard X-ray emission observed in AXPs has also been proposed to arise from the twisted magnetosphere, which is thought to act as an accelerator and create a hot corona close to the surface of the star (Thompson & Beloborodov 2005; Beloborodov & Thompson 2007). In this case, we would expect the changes seen here (mainly those associated with the onset of bursts) to have corresponding changes at hard X-rays. den Hartog et al. (2007) report no variability within measurement errors for various observations carried out before 2006. No measurements after the recent burst activity are reported and establishing/constraining any associated variability would be of interest.

The origin of the optical and IR emission in the magnetar model is not well understood, with the proposed mechanisms not studied in detail and thus having uncertain correlation with the X-ray flux (see Thompson & Beloborodov 2005). We find no significant change in the near-IR flux after the bursts that could be correlated with the overall increase in the X-ray flux during this time. However, given the large variability seen from 4U 0142+61 in the optical/IR and the subtle nature of the changes in X-rays, we cannot test for a possible correlation between the emission at these wavelengths.

6.2. The Disk Models

The discovery of mid-IR emission from a possible disk around 4U 0142+61 has prompted debate as to whether it is a passive (Wang et al. 2006) or an active disk (Ertan et al. 2007a). In the case of a passive disk the magnetar mechanism is still needed to explain the X-ray emission from the star, while an active disk accretes onto a star with a dipole field of $\sim 10^{12-13}$ G (a magnetar field in the quadrupole or higher components in then needed to explain the bursting behavior; Ertan et al. 2007b,a). The (unpulsed) optical/IR/UV emission results from the disk as it radiates through viscous energy dissipation and by irradiation from the star. Most of the disk radiation, which peaks in the IR, comes from the outer regions.

The fact that the main spectral changes are seen to correlate with an increased burst activity argue against a disk origin. Although an increased X-ray flux from the star can affect the irradiation emission from the putative disk around 4U 0142+61, these X-ray changes might or might not be accompanied by changes at longer wavelengths depending on the reprocessing efficiency

of the disk. As the X-ray flux is still observed to be higher in the last observation, changes in the optical/IR might be present. However, the large range of previously reported IR fluxes do not allow for intrinsic changes in the emission of several percent, as observed in the X-ray range, to be readily identified.

7. CONCLUSION

The observations presented here further demonstrate that variability in AXPs is common. The variability takes many forms and proceeds on a wide range of time scales. The radiative properties of these objects are seen to vary by orders of magnitude in the case of outbursts and by a few percent as seen here. The pulse profile and pulsed fraction of 4U 0142+61 have undergone evident changes during the span of our observations (2000–2007). Before the bursts were detected the pulse profile became more sinusoidal, while more complicated changes were seen afterwards. On the other hand, the pulsed fraction has increased throughout the observations. The total flux is observed to have been nearly constant in the observations taken before the bursts, while an increase of $\sim 10\%$ is seen afterwards in the 0.5–10 keV range. The flux increase is energy dependent, with higher energies showing a larger increase. No evidence for further changes as a direct consequence of the bursting activity is seen. The data also suggest a correlation between flux and hardness of the spectrum, with larger fluxes on average having harder spectra. In general, the spectral behavior of the source supports a magnetar origin, where current models predict that larger twists in the magnetosphere produce brighter, harder emission which can

coincide with increased burst activity. However, the detailed evolution of the spectrum and pulse characteristics throughout the observations suggests a more complicated scenario, with multiple mechanisms interacting to produce the observed properties. No significant variations in the near-IR emission from the source are detected, consistent with the few percent change observed in the X-rays flux and uncertainties on how the proposed disk around 4U 0142+61 would respond to this change.

Based on observations obtained at the Gemini Observatory (Program IDs GN-2006A-DD-7 and GN-2007A-DD-1), which is operated by the Association of Universities for Research in Astronomy, Inc., under a cooperative agreement with the NSF on behalf of the Gemini partnership: the National Science Foundation (United States), the Particle Physics and Astronomy Research Council (United Kingdom), the National Research Council (Canada), CONICYT (Chile), the Australian Research Council (Australia), CNPq (Brazil) and CONICET (Argentina). This research has made use of data obtained through the High Energy Astrophysics Science Archive Research Center Online Service, provided by the NASA/Goddard Space Flight Center. FPG is supported by the NASA Postdoctoral Program administered by Oak Ridge Associated Universities at NASA Goddard Space Flight Center. This work was also supported by the NSERC Discovery Program, FQRNT, the Canada Foundation for Innovation, and an R. Howard Webster Fellowship of the Canadian Institute for Advanced Research to VMK.

REFERENCES

- Alpar, M. A. 2001, *ApJ*, 554, 1245
 Beloborodov, A. M., & Thompson, C. 2007, *ApJ*, 657, 967
 Bhattacharya, D., & Soni, V. 2007, *ArXiv e-prints*, 705
 Campana, S., et al. 2007, *A&A*, 463, 1047
 Chatterjee, P., Hernquist, L., & Narayan, R. 2000, *ApJ*, 534, 373
 den Hartog, P. R., et al. 2007, *Ap&SS*, 308, 647
 Dhillon, V. S., et al. 2005, *MNRAS*, 363, 609
 Dib, R., Kaspi, V., Gavriil, F., & Woods, P. 2006, *The Astronomer's Telegram*, 845, 1
 Dib, R., Kaspi, V. M., & Gavriil, F. P. 2007, *ApJ*, in press
 Dib, R., Kaspi, V. M., & Gavriil, F. P. 2007, *ApJ*, submitted (*astro-ph/0706.4156*)
 Durant, M., & van Kerkwijk, M. H. 2006a, *ApJ*, 650, 1070
 Durant, M., & van Kerkwijk, M. H. 2006b, *ApJ*, 650, 1082
 Durant, M., & van Kerkwijk, M. H. 2006c, *ApJ*, 652, 576
 Ertan, Ü., et al. 2007a, *Ap&SS*, 308, 73
 Ertan, Ü., Erkut, M. H., Ekşi, K. Y., & Alpar, M. A. 2007b, *ApJ*, 657, 441
 Fernández, R., & Thompson, C. 2007, *ApJ*, 660, 615
 Gavriil, F. P., Dib, R., Kaspi, V. M., & Woods, P. M. 2007a, *The Astronomer's Telegram*, 993, 1
 Gavriil, F. P., Dib, R., Kaspi, V. M., & Woods, P. M. 2007b, *ApJ*, in preparation
 Gavriil, F. P., & Kaspi, V. M. 2002, *ApJ*, 567, 1067
 Gavriil, F. P., & Kaspi, V. M. 2004, *ApJ*, 609, L67
 Gotthelf, E. V., & Halpern, J. P. 2007, *Ap&SS*, 308, 79
 Güver, T., Özel, F., & Göğüş, E. 2007, *ApJ*, submitted (*astro-ph/0705.3982*)
 Güver, T., Özel, F., Göğüş, E., & Kouveliotou, C. 2007, *ApJ*, submitted (*astro-ph/0705.3713*)
 Hulleman, F., et al. 2001, *ApJ*, 563, L49
 Hulleman, F., van Kerkwijk, M. H., & Kulkarni, S. R. 2004, *A&A*, 416, 1037
 Israel, G. L., et al. 2003, *ApJ*, 589, L93
 Israel, G. L., Mereghetti, S., & Stella, L. 1994, *ApJ*, 433, L25
 Juett, A. M., Marshall, H. L., Chakrabarty, D., & Schulz, N. S. 2002, *ApJ*, 568, L31
 Kaspi, V. M. 2007, *Ap&SS*, 308, 1
 Kaspi, V. M., Dib, R., & Gavriil, F. P. 2006, *The Astronomer's Telegram*, 794, 1
 Kaspi, V. M., et al. 2003, *ApJ*, 588, L93
 Kaspi, V. M., Roberts, M. S. E., & Harding, A. K. 2006, *Isolated neutron stars*, ed. W. H. G. Lewin & M. van der Klis (Cambridge University Press, UK: Compact stellar X-ray sources), 279
 Kern, B., & Martin, C. 2002, *Nature*, 415, 527
 Kuiper, L., Hermsen, W., den Hartog, P., & Collmar, W. 2006, *ApJ*, 645, 556
 Lyutikov, M., & Gavriil, F. P. 2006, *MNRAS*, 368, 690
 Molkov, S. V., et al. 2004, *Sov. Astron. Lett.*, 30, 534
 Özel, F., & Güver, T. 2007, *ApJ*, 659, L141
 Patel, S. K., et al. 2003, *ApJ*, 587, 367
 Rea, N., et al. 2007a, *MNRAS*, in press (*astro-ph/0707.3363*)
 Rea, N., et al. 2007b, *ApJ*, submitted (*astro-ph/0703128*)
 Tam, C. R., Kaspi, V. M., Gavriil, F. P., & Dib, R. 2007, *ApJ*, submitted (*astro-ph/0707.2093*)
 Thompson, C., & Beloborodov, A. M. 2005, *apj*, 634, 565
 Thompson, C., & Duncan, R. C. 1995, *MNRAS*, 275, 255
 Thompson, C., & Duncan, R. C. 1996, *ApJ*, 473, 322
 Thompson, C., Lyutikov, M., & Kulkarni, S. R. 2002, *ApJ*, 574, 332
 Tiengo, A., et al. 2005, *A&A*, 437, 997
 Turner, M. J. L., et al. 2001, *A&A*, 365, L27
 Wang, Z., Chakrabarty, D., & Kaplan, D. L. 2006, *Nature*, 440, 772
 Woods, P. M., et al. 2004, *ApJ*, 605, 378
 Woods, P. M., & Thompson, C. 2006, in *Compact Stellar X-ray Sources*, ed. W. H. G. Lewin & M. van der Klis (Cambridge: CUP), 547